Original Article

New approach for calibration of pixelated scintillation detectors of intraoperative gamma cameras

Afshin Akbarzadeh[1, 2], Valiallah Saba[2], Mohammad Reza Ay[3]

[1]Research Center for Molecular and Cellular Imaging, Tehran University of Medical Sciences, Tehran, Iran
[2]Radiation Research Center, Faculty of Paramedicine, AJA University of Medical Sciences, Tehran, Iran
[3]Department of Medical Physics and Biomedical Engineering, Tehran University of Medical Sciences, Tehran, Iran

(Received 18 May 2016, Revised 3 July 2016, Accepted 5 July 2016)

ABSTRACT

Introduction: SURGEOSIGHT is a dedicated intra-operative hand-held gamma camera designed and manufactured by our team to be used for lymphoscintigraphy. Although conventional gamma cameras are widely used, they lack the capability of the sentinel lymph node (SLN) imaging in the operation room. Like conventional gamma cameras it is necessary to calibrate SURGEOSIGHT for linearity distortion, energy and flood correction. Our main objective in this study is to develop and implement three techniques for linearity, energy and uniformity corrections.

Methods: The camera is made up of a pixelated cesium iodide (sodium-activated) (CsI(Na)) scintillation crystal with 1×1 mm^2 element size along with a Hamamatsu H8500 flat-panel multi-anode (64 channels) photomultiplier tube. All triple corrections required lookup tables (LUTs). To generate all three LUTs, one uncalibrated acquisition is necessary. Linearity distortion correction was based on localization of physical pixels of crystal and thin plate spline interpolation to estimate the amount of distortion. Energy correction LUT was simply a photo-peak map of incoming events which was estimated using self-organizing map technique.

Results: The results showed improvements qualitatively and quantitatively. The extrinsic energy resolution was enhanced from 50% to about 20.6%. Integral uniformity and the differential uniformity, after uniformity correction, in useful field-of-view (UFOV) was measured 9.5% and 4.5%, respectively.

Conclusion: Results substantiated that the correction techniques guarantee uniform and accurate output of the SURGEOSIGHT which is desirable for intra-operative localization of the sentinel lymph nodes in breast cancer and also for imaging of other superficial tumors.

Key words: Uniformity correction; Energy correction; Linearity distortion correction; Self-organizing map; Intra-operative gamma camera

Iran J Nucl Med 2017;25(1):34-42
Published: January, 2017
http://irjnm.tums.ac.ir

Corresponding author: Valiallah Saba, Radiation Research Center, Faculty of Paramedicine, AJA University of Medical Sciences, Etemadzade Ave., Fatemi St., Tehran, Iran. E-mail: vsaba@aut.ac.ir

INTRODUCTION

Nuclear medicine imaging introduces a non-invasive method to collect functional information at the molecular and cellular level that plays an important role to the determination of health status by measuring the uptake and turnover of target-specific radiotracers in tissue [1, 2]. The field offers a broad array of tools for assessment of normal and diseased tissues. The most prevalent tools in this area are imaging and non-imaging gamma detectors which accumulate events or counts of detected gamma photons.

Compact intra-operative gamma imagers are miniaturized version of typical gamma cameras invented by Hal Anger. The standard gamma cameras are not practical imaging devices for radio-guided surgery. The remarkably large detector head of a standard gamma camera are not suitable for operation at surgical sites e.g. breast and inherently accepts background activity from other organs resulting non-optimal spatial resolution, lower image contrast, and limited quality in breast imaging. Moreover, collimator sensitivity, large detector separation and relatively coarse detector elements in standard gamma camera system leads to limited sensitivity and spatial resolution for intra-operative imaging. Finally, the relatively high cost (time and staff) per study using standard nuclear imaging systems limits their practicality for intra-operative use.

On the contrary, a compact imager offers certain ideal capabilities such as flexibility, convenience and multiple-orientation positioning. This type of imagers enables the user to bring the detector head in close contact with the breast for the least proximity imaging, which gains optimal spatial resolution and higher sensitivity. Besides, the facilitated detector head positioning leads to reduction or elimination of the background activity from adjacent organs, such as the heart.

Intraoperative compact gamma imagers and gamma cameras are structurally identical in principles. Therefore the same technical challenges have to be met. Standard gamma camera has been ceaselessly optimized since its introduction in 1958 [3]. However, there still exist well known intrinsic constraints due to the manufacturing process as well as the physical characteristics, such as low spatial resolution, linearity and spatial distortion, or energy non-uniformity across the face of the crystal.

Several known techniques have been introduced for calculation of the interaction position in gamma cameras of which the Anger method is more commonplace [3-9]. Position calculation techniques determine the interaction position based on positions of the PMTs consequently bringing about several problems. The sensitivity of PMTs is not identical, varies temporally also not uniform in different angles which causes a calculated position tends to shift towards the position of the most sensitive PMT. Moreover, a certain number of photons is lost at crystal margins, either by escaping the crystal or by lack of PMTs to surround the interaction position. In addition, crystal sensitivity to gamma radiation is non-uniform. The results of these factors lead to spatial distortion and energy non-uniformity.

“Triple correction” is a prevailing methodology for calibration of typical gamma cameras [7, 10-16] which includes spatial distortion correction [17-19] (also called linearity correction), energy correction [20-23] and uniformity correction (also called flood correction) [24, 25]. Although pixelated gamma cameras are slightly different with typical Anger cameras, the story of non-uniformity and spatial distortion is the same, makes it necessary to apply triple correction for these type of cameras as well [13].

There is thus, a necessity for simple and fast calibration method to be performed by the final user in assembled dedicated compact cameras. Recently our team has developed an intra-operative compact gamma camera, SERGEOSIGHT [26], for intra operative use. The main goal of this work is to develop a relatively new simplified calibration procedure optimized for compact gamma cameras with pixelated crystal. This paper describes details of triple corrections for newly developed gamma camera: linearity correction based on thin plate spline, the energy calibration procedure based on trained Kohonen network which is well known as "self-organizing map" and uniformity correction based on random number generation.

METHODS

System description

SURGEOSIGHT includes a low-energy general-purpose parallel-hole lead collimator, a 43×43 array of sodium activated cesium iodide (CsI(Na)) scintillator crystal and H8500C Position sensitive photomultiplier tube (PSPMT) (Hamamatsu Photonic Co., Japan) (Figure 1).

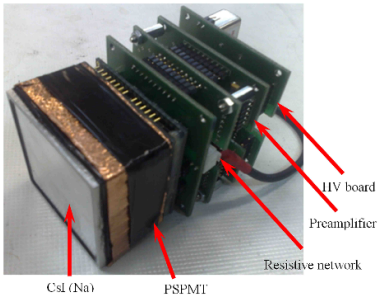

Fig 1. Electronic readout for the manufactured gamma camera.

The collimator holds 1.2 mm hexagonal holes, 18 mm thickness, and 0.2 mm septal thickness. The crystal is pixelated with pixel dimensions of 1×1×5 mm^3 (1.2 mm pixel pitch) and the size of active area for PSPMT is 49×49 mm^2. Detector data acquisition and processing required a dedicated electronics which was designed and implemented by our team [26-28].

Data acquisition

The PSPMT produces 8×8 anode signals ($X_{1...8}$and $Y_{1...8}$), that are used to calculate four position signals (X^+, X^-, Y^+ and Y^-). These position signals are calculated using weighted sum of all 64 anode signals based on Anger logic and passed to the acquisition board. Eventually, the digital position values of the incident photon are transferred via LAN cable to a computer to be stored as List Mode Format (LMF) data.

Our calibration approach is based on acquired uncalibrated data. SURGEOSIGHT software is capable of recording the incoming data stream on a file. The data stream is raw output of PSPMT which contains above mentioned four digital position values. This type of data acquisition is advantageous in a way that only one data acquisition is necessary for all three corrections and the recorded list-mode data can be used several times to perform all corrections. For list-mode acquisition a flood-field phantom (50×50×5 mm^3) was filled with a uniform solution of Tc-99m. This phantom was placed in direct contact with the collimator.

Linearity correction

It is known fact that spatial non-linearity is the direct consequence of intrinsic shortcomings in positioning algorithm which maps the output of PSPMT on the crystal surface. This phenomenon distorts the straight lines into wavy lines and makes the image seem inflated around each PMT. Figure 2a schematically shows the way that non-linear image is formed for each PMT. In order to correct the non-linearity of the distorted image one could take the advantage of image warping algorithms (Figures 2c and 2d).

Since SURGEOSIGHT uses a pixelated crystal, the uncalibrated image of uniform flood source (without any correction and wide energy window) will appear as irregular grid of spots in which each spot represents a physical pixel of crystal (Figures 2a and 5a). The linearity correction will be accomplished by non-rigid mapping of this uncalibrated image on a regular grid of the same size.

Measurement phase: There are three main steps to obtain linearity correction lookup table: (1) detection of spots on irregular grid of physical pixels of crystal, (2) calculation of delta vector for every spot. The delta vector is a two dimensional x-y vector which is required to correct the position of a spot. (3) Thin plate spline interpolation of the vectors to make up linearity correction LUTs.

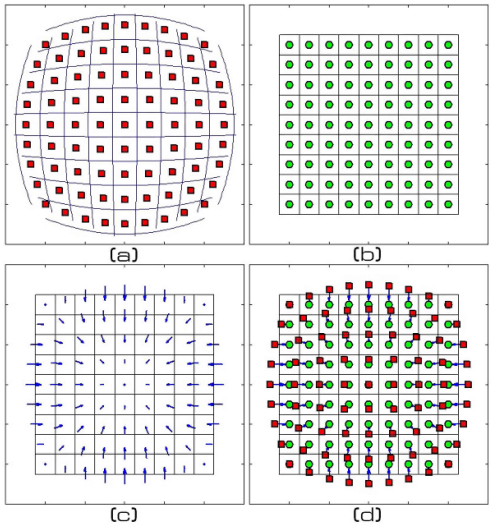

Fig 2. schematic explanation for linearity correction process (a)inflated configuration for non-regular grid and spots as the output of single PMT (b) regular grid as target of linearity correction process (c) Calculated vector field to transform a into b (d) transformation.

Stage 1: The first stage includes a set of procedures for detection of precise location of each spot on the output mage. First of all, the spots are initially detected using a watershed [29] algorithm. In the next step, detected positions are shown to the user by means of an interactive GUI containing a set of graphic tools for correction of probable mis-detections (Figure 3).

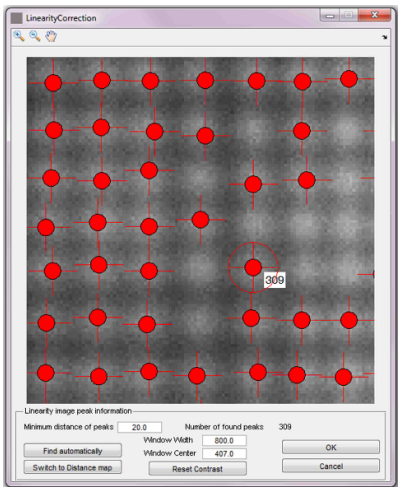

Fig 3. The interactive UI for semiautomatic peak selection.

Stage 2: the centroid for each detected spot is calculated to give the exact location of spot peak which is equivalent to a center of single element of a non-regular grid. Every element of non-regular grid corresponds to which of regular grid of the same size. The Delta Vector is a vector which assigns the elements of non-regular grid to regular grid.

Stage 3: in order to construct vector field it is necessary to compute delta vector for any tiny location on the detector surface. The solution is to take advantage of an appropriate 2D interpolation method which fits with intrinsic nature of irregularity. Thin plate spline (TPS) interpolation [30] is an interpolation approach which is introduced to interpolate irregular scattered data in a very smooth manner.

TPS interpolation method: Given a set of non-collinear 2D paired control points $\{(x_i, y_i), (\Delta X_i, \Delta Y_i) : i = 1, \cdots, N\}$ in which ΔX_i and ΔY_i are the *xy* element of ith vector. It is often desirable to estimate corresponding function values for the node points of a regular grid. There exist many approaches to solve this problem (e.g., bilinear interpolation and triangulation techniques) but the smoothest possible real-valued function *f* is thin plate spline.

Let :

$$\Delta X_i = f_x(x_i, y_i) \quad (1)$$

$$\Delta Y_i = f_y(x_i, y_i) \quad (2)$$

and suppose that the smoothness is estimated by:

$$Smoothness(f) = \iint_{R^2} \left(\frac{\partial^2 f}{\partial x^2}\right) + 2\left(\frac{\partial^2 f}{\partial x \partial y}\right) + \left(\frac{\partial^2 f}{\partial y^2}\right) dxdy \quad (3)$$

It has been proved that the variation problem of minimizing (Eq3) under the interpolation conditions (Eq1) and (Eq2) is solved uniquely by a thin plate spline (TPS) of the form

$$f(x, y) = A_1 + A_2 x + A_3 y + \sum_{i=1}^{N} F_i r_i^2 ln(r_i^2) \quad (4)$$

$$r_i^2 = (x - x_i)^2 + (y - y_i)^2 + d^2 \quad (5)$$

Where A_0, A_1 and A_2 are the coefficients of the planar term of the spline, F_i is the coefficient for the i^{th} spline term and parameter d^2 acts like a stiffness parameter. As d^2 goes up, TPS produces a stiffer (smoother) surface. Besides, the smoothness in (Eq3) is finite if and only if F_is have the property that

$$\sum_{i=0}^{N} F_i = 0 \quad (6)$$

$$\sum_{i=0}^{N} x_i F_i = 0 \quad (7)$$

$$\sum_{i=0}^{N} y_i F_i = 0 \quad (8)$$

Now there are *N+3* equations and *N+3* unknown coefficients which make a linear system of equations. For 2D interpolation of scattered control points, two linear equation systems in form of (Eq6) and (Eq7) must be solved to yield the *2× (N+3)* unknown coefficients.

$$\begin{bmatrix} 1 & x_1 & y_1 & U_{11} & \cdots & U_{1N} \\ & & \vdots & & \ddots & \vdots \\ 1 & x_N & y_N & U_{N1} & & U_{NN} \\ 0 & 0 & 0 & 1 & \cdots & 1 \\ 0 & 0 & 0 & x_1 & & x_N \\ 0 & 0 & 0 & y_1 & & y_N \end{bmatrix} \times \begin{bmatrix} A_{x1} \\ A_{x2} \\ A_{x3} \\ F_{x1} \\ \vdots \\ F_{xN} \end{bmatrix} = \begin{bmatrix} \Delta X_1 \\ \vdots \\ \Delta X_N \\ 0 \\ 0 \\ 0 \end{bmatrix} \quad (9)$$

$$\begin{bmatrix} 1 & x_1 & y_1 & U_{11} & \cdots & U_{1N} \\ & & \vdots & & \ddots & \vdots \\ 1 & x_N & y_N & U_{N1} & & U_{NN} \\ 0 & 0 & 0 & 1 & \cdots & 1 \\ 0 & 0 & 0 & x_1 & & x_N \\ 0 & 0 & 0 & y_1 & & y_N \end{bmatrix} \times \begin{bmatrix} A_{y1} \\ A_{y2} \\ A_{y3} \\ F_{y1} \\ \vdots \\ F_{yN} \end{bmatrix} = \begin{bmatrix} \Delta Y_1 \\ \vdots \\ \Delta Y_N \\ 0 \\ 0 \\ 0 \end{bmatrix} \quad (10)$$

Where:

$$U_{ij} = \left[(x_j - x_i)^2 + (y_j - y_i)^2 + d^2\right] \times \ln((x_j - x_i)^2 + (y_j - y_i)^2 + d^2) \quad (11)$$

Once unknown coefficients are obtained, one can use the function f(x,y) to calculate vector field for node points of a regular grid. In our implementation there were N=34×34 control points which made up two linear system matrices of 1159×1159.

The calculated vector field is stored inside two independent LUTs (x-LUT and y-LUT) one holding the x element and the other holding y element of each vector.

Correction phase: In order to correct linearity for any incoming event, first of all the location of event is estimated from positioning algorithm. Then the x and y elements of vector are calculated from the corresponding location in x-LUT and y-LUT using bilinear interpolation. The true location is estimated by shifting the position towards the calculated vector from LUTs.

Energy correction

It is well known that, gamma camera sensitivity to the energy of an incident gamma photon is not uniform, i.e. maximum energy (photo-peak) in an energy spectrum for detected events varies with position of the incident gamma photon. Moreover, the width of the spectrum peak (i.e., energy resolution) is not uniform as well. The conventional energy correction techniques rely on the partial measurement of photo-peak on different regions of FOV. The generated photo-peak map is used to correct energy of incident photon to every small region either by shift of all photons energy with respect to a reference small region or by multiplication of a correction factor. To implement this approach every physical pixel of SURGEOSIGHT was supposed to construct energy spectrum independently. Figure 4 shows a schematic 3D array which is being used for partial spectrum acquisition. This method is prohibitive in term of memory and performance.

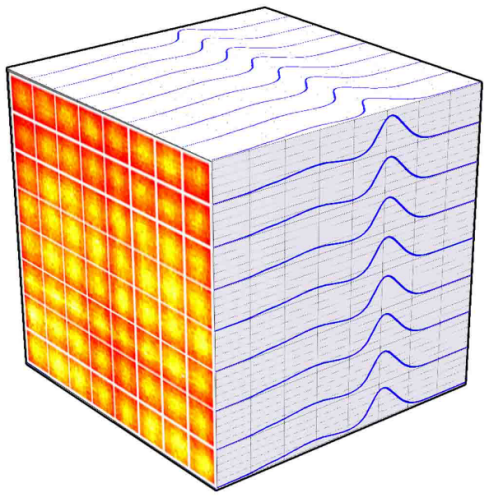

Fig 4. Schematic view (for 8×8 array) of conventional data acquisition for energy correction using 3D array of energy bins.

Measurement phase: SOM (Self organizing map) or Kohonen networks [31] are a type of artificial neural network which are trained to generate discretized representation of the input space of the training samples as a map. SOM convergence is proved theoretically [32] and convergence criteria are based on measures performed on the map itself, evaluating where pairs of training data fall on the map with relation to each other [33]. The measurement on the map itself, in order to measure the stability or convergence of a map is a common practice [34, 35]. It is supposed that SOMs are capable of producing photo-peak map for energy correction [36].

Assume that map consists of M×N neurons located on a regular two dimensional rectangular grid. Each neuron $C_{i,j}$ is represented by a weight $E_{i,j}$ as the photo-peak. All neurons were initialized to 140 KeV for technetium. The training phase takes the advantage of competitive learning. When an incident photon is fed to SOM lattice, the neuron $C_{i,j}$ whose indices are most close to the location of input photon is called the best matching unit (BMU). The difference of photon energy and current E_{ij} is calculated as a ΔE_{ij}. The weights of the BMU and its neighbors in the SOM lattice are modified by calculation of ΔE_{ij}. The magnitude of the modification decreases with count and distance of neighbors from the BMU. The the following relations show the update formula for a neuron $C_{i,j}$ with weight vector $E_{i,j}$:

$$\text{Time Factor} = e^{-\alpha c} \quad (12)$$

$$\text{Distance Factor} = e^{-\frac{r^2}{2(\alpha c)^2}} \quad (13)$$

$$E_{i,j}(itr+1) = E_{i,j}(itr) + \text{Time Factor} \times \text{Distance Factor} \times \Delta E_{i,j} \quad (14)$$

Where α is a constant that obtained experimentally, r is Euclidian distance of neighbors from the BMU and c represents count. Generally the convergence speed depends on the SOM grid size and the energy spectrum of incident photon. As a rule of thumb in our implementation the convergence occurs in about 40 counts per pixel. For a photo-peak map of 34×34 it converges around 50K count and for 512×512 the SOM usually converges on 10 million counts. The obtained photo-peaks are normalized to reference photo-peak and the result is saved in energy correction LUT.

Correction Phase: The generated LUT which includes the photo peak correction factors was saved in the measurement phase. In order to correct the energy one could find the location of any incoming events and find the energy correction factor from the corresponding location in energy correction LUT using the bilinear interpolation method.

Uniformity correction

Uniformity or flood correction is the last calibration which guarantees a uniform flood source will produce a uniform image.

Measurement phase: In order to perform uniformity correction the recorded list-mode data were read and linearity correction and energy correction were applied. The resulting image was normalized to the average pixel count to calculate the uniformity LUT.

Correction phase: In uniformity correction phase, each event in pixel (i,j) holds a corresponding uniformity correction factor inside uniformity LUT, which compensates the slight non-uniformities by intensifying or suppressing the corresponding counts for incoming events on that pixel.

The correction factor is separated into integer part and decimal part. The integer part manifolds the register count of event. For decimal part, a random number is generated. Then event will be suppressed if the random number was less than the decimal part and vice versa.

Evaluations

Generally energy correction improves the energy resolution of system. Therefore in order to evaluate the effect of energy correction, the energy resolution was calculated. A flood-field phantom (50×50×5 mm^3) filled with a uniform solution of Tc-99m (500 μCi) was used to expose the detector while the collimator was installed. The FWHM of photo-peak of the energy spectrum was calculated using Gaussian curve fitting with and without energy correction.

The same flood-field source which was placed in direct contact with collimator used to quantify the

system uniformity. According to National Electrical Manufacturers Association (NEMA) NU1-2007 standards [37] the integral and differential uniformity values were computed inside central FOV (CFOV) and useful FOV (UFOV) which is smoothed with a Gaussian 3×3 kernel. UFOV is the FOV whose marginal pixels are removed, whereas the CFOV is described in NEMA standard. Integral uniformity was specified as the difference between minimum and maximum intensity of flood image over the sum of minimum and maximum intensity of flood image (Eq15). Differential uniformity was specified as the largest difference between two pixels within any set of three contiguous pixels in a row or column of the flood-field image.

$$Uniformity = \frac{max-min}{max+min} \times 100\% \qquad (15)$$

RESULTS

Linearity correction

For linearity correction procedure, a previously recorded list-mode data was read out with no calibration. Figure 5c shows the calculated vector field for the resulted uncalibrated image. The calculated vector field was interpolated using TPS and the Linearity calibration factors were saved on two LUT files which were used to correct the uncalibrated data (Figure 6).

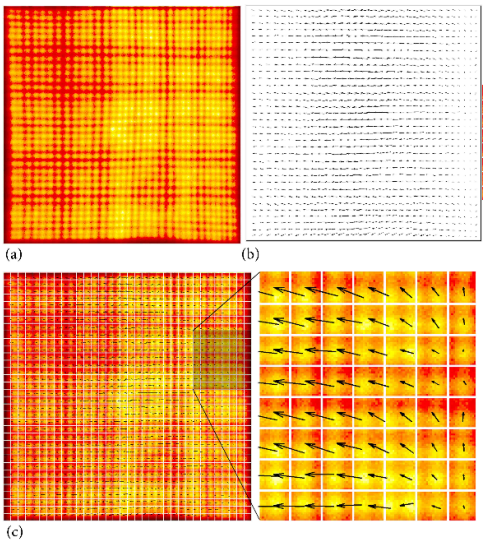

Fig 5. Calculated vector fields for linearity correction (a) primary image with no calibration (b) the calculated vector field (c) vector field, primary image and regular grid altogether.

Energy correction

After linearity correction, it is necessary to correct the energy of linearity-corrected photons. A map of photo-peak is needed to correct the energy of events to specific incident location which was produced using SOM.

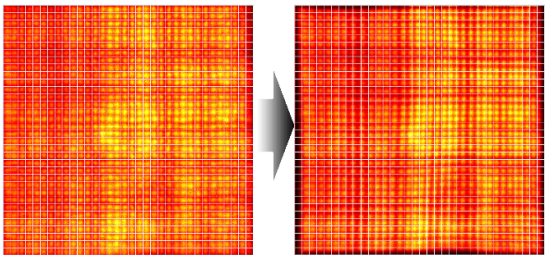

Fig 6. Linearity correction based on image warp under vector fields and TPS interpolation.

Figure 7 indicates the convergence of SOM to produce photo-peak map for different counts. The map was initialized to 140 KeV which is appropriate for technetium and after 8×10^6 counts 512×512 map was converged.

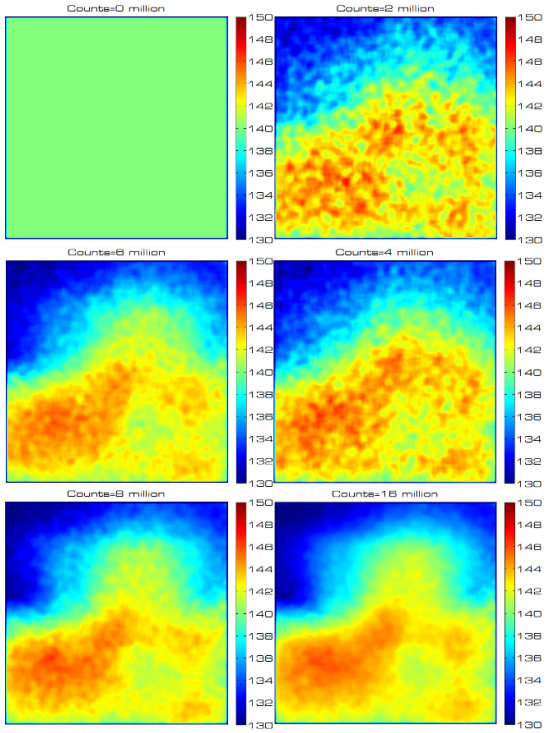

Fig 7. Convergence behavior of the SOM representing the photo-peak (KeV) map for technetium to make the lookup table for energy correction.

The calculated map was compared with conventional method which is shown in Figure 8. The extrinsic energy resolution was measured about 50.0% and 20.6% at Tc-99m photon energy before and after energy correction, respectively.

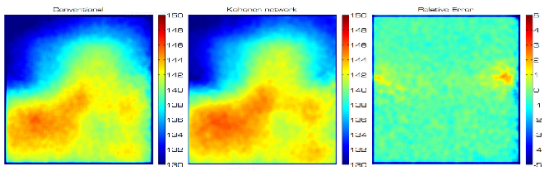

Fig 8. Comparison of obtained photo-peak map from conventional and Kohonen-network techniques.

Uniformity correction

Uniformity correction is the last step in triple corrections that guarantees the uniform output of detector. Figure 9 indicates the effect of uniformity correction on a flood source which leads to a uniform flood image. The images show the improvement of the image uniformity after uniformity correction. The integral and differential uniformity values were calculated based on the flood-field images. Table 1 shows the calculated values for integral and differential uniformities.

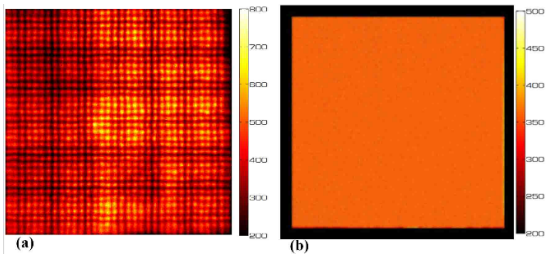

Fig 9. Effect of uniformity correction on flood source (a) without uniformity correction (b) with uniformity correction.

Table 1: Uniformity analysis before and after uniformity correction (UC: uniformity correction, IU: integral uniformity, DU: differential uniformity, CFOV: central field of view, UFOV: useful field if view).

	Without UC		With UC	
	CFOV	**UFOV**	**CFOV**	**UFOV**
IU (%)	54.0	55.4	9.5	4.5
DU (%)	26.9	19.4	7.6	4.5

DISCUSSION

The SERGEOSIGHT is a new gamma camera designed as a dedicated imager for the preoperative and intraoperative scintigraphy [26]. This study attempted to design and implement three main calibration procedures for our newly-developed mini gamma camera. Each calibration included two separate phases; acquisition in order to compute LUTs and correction of incoming events using LUTs.

Our implemented linearity method was mainly based on accurate detection of spots center representing the physical pixels of pixelated crystal. Although we attempted to automate this process using water shed segmentation algorithm, in certain cases due to noise the algorithm failed to find correct location of the spots. In these circumstances the user is supposed to correct the inaccuracies. In the next stage for interpolation of vector field we took the advantage of TPS which is a well-known irregular interpolation method in image warping field. However, there are other methods for 2D irregular interpolation which could be used as substitute.

We implemented two different techniques to produce photo-peak map of detector to calibrate the energy. The minimum number for M and N (number of neurons for SOM) is supposed to be physical dimensions of pixelated crystal (34×34). The bigger sizes are possible in order to support subpixel resolutions. In this work we supposed the M=N=512, which was considered to be identical to the size of linearity correction table to facilitate the correction phase for subpixel count distribution. Conventional method for energy correction is more resource wasting in terms of memory and performance compared to SOM method. Clearly speaking, to construct a typical map of size M×N containing spectrums with 128 bins an integer 3D array of M×N×128 is required. On the contrary SOM method requires less memory than conventional method. The conventional method is applicable conveniently in general hardware and OS available in the market. The problem with the conventional method will emerge in the cases of dedicated hardware and embedded OS. It is imaginable that one could make the whole intraoperative gamma imager more compact with smaller monitor and processor. In this case the resource saving algorithms are the only option. As Figure 7 shows the SOM converges in 7-8×10^6 counts for 512×512 photo-peak map. For lower sizes of map the convergence will occur faster. The comparison of two maps showed low relative error (under 5%) which makes the SOM method as an appropriate proxy for conventional method. Despite the fact that SOM has been addressed in monolithic crystal calibrations [12, 36], it has not been utilized in pixelated crystals yet. Applying energy correction improved the system extrinsic energy resolution from50% to 20.6% at Tc-99m photon energy. It is clear that the energy resolution of pixelated detectors depends mainly on both pixel size and also intrinsic efficiency of the crystal material. In fact there is a remarkable amount of light loss in detector pixel elements which deteriorates energy resolution in pixelated crystals. Consequently this configuration of small gamma cameras often has a FWHM energy resolution worse than single crystal scintillation cameras [38-41].

Uniformity correction has considerably improved the system uniformity. The improvement can be observed visually in Figure 9. Quantitatively speaking, system differential uniformity value after

correction was obtained 4.5% in both of the UFOV and the CFOV (Table 1). Besides the integral uniformity after correction became 9.5% and 7.7% for the UFOV and CFOV, respectively. The uniformity values are comparable with those reported in the literature [7, 8, 42].

CONCLUSION

Triple corrections (linearity correction, energy correction and uniformity correction) are the most important procedure in gamma cameras which guarantee the uniform output of these imagers. We especially designed and implemented all three procedures for our newly designed intra-operative hand-held gamma imager to improve its uniformity and energy resolution. Particularly our proposed SOM-based technique for energy correction is simple, fast and needs less memory than conventional methods for energy calibration which is a perfect alternative for compact imagers with limited memory resources. SURGEOSIGHT is a newly introduced camera by our team, uniquely designed compact camera for localization of radioactive SNLs in the head and neck and other different anatomic locations providing spatial information that can help to discriminate focal uptake against diffuse background activity.

REFERENCES

1. Bischof Delaloye A. Progress in the diagnosis and treatment of disease by nuclear medicine and molecular imaging: highlights of the European Association of Nuclear Medicine Congress, Naples 2001. Eur J Nucl Med Mol Imaging. 2002 Jan;29(1):139-59.
2. Nishimura T. Angina pectoris: progress in diagnosis and treatment. II. Progress in imaging diagnosis. 2. The role of nuclear medicine. Nihon Naika Gakkai Zasshi. 1997 Feb 10;86(2):214-9.
3. Anger HO. Scintillation camera. Rev. Sci. Instrum. 1958;29(1):27-33.
4. Gray RM, Macovski A. Maximum a posteriori estimation of position in scintillation cameras. IEEE Trans Nucl Sci. 1976;23(1):849-52.
5. Barrett HH, Hunter WC, Miller BW, Moore SK, Chen Y, Furenlid LR. Maximum-likelihood methods for processing signals from gamma-ray detectors. IEEE Trans Nucl Sci. 2009 Jun 1;56(3):725.
6. Bruyndonckx P, Leonard S, Tavernier S, Lemaitre C, Devroede O, Wu Y, et al. Neural network-based position estimators for PET detectors using monolithic LSO blocks. IEEE Trans Nucl Sci. 2004;51(5):2520-5.
7. Jeong MH, Choi Y, Chung YH, Song TY, Jung JH, Hong KJ, Min BJ, Choe YS, Lee KH, Kim BT. Position mapping, energy calibration, and flood correction improve the performances of small gamma camera using PSPMT. IEEE Nucl Sci Symp Conf Rec. 19-25 October 2003.
8. Jeong MH, Choi Y, Chung YH, Song TY, Jung JH, Hong KJ, Min BJ, Choe YS, Lee KH, Kim BT. Performance improvement of small gamma camera using NaI(Tl) plate and position sensitive photo-multiplier tubes. Phys Med Biol. 2004 Nov 7;49(21):4961-70.
9. Hung N, Joung J, Lee K, Kim Y. Development of correction schemes for a small field of view gamma camera. Biomed Eng Lett. 2012;2(4):215-22.
10. Inbar D, Gafni G, Grimberg E, Koren J. Gamma camera correction system and method for using the same. Patent US4588897 A. 1986.
11. Berlad G, Wainer N. Gamma camera with two sequential correction maps. Patent US6559450 B1. 2003.
12. España S, Deprez K, Van Holen R, Vandenberghe S. Fast calibration of SPECT monolithic scintillation detectors using un-collimated sources. Phys Med Biol. 2013 Jul 21;58(14):4807-25.
13. Thanasas D, Maintas D, Georgiou E, Giokaris N, Karabarbounis A, Papanicolas CN, Stiliaris E. Correcting spatial distortion and non-uniformity in planar images from γ-Camera systems. IEEE Nucl Sci Symp Conf Rec. 19-25 October 2008.
14. Knoll GF, Strange DR, Bennett MC. Radiation signal processing system. Patent US4212061 A. 1980.
15. Muehllehner G, Colsher JG, Stoub EW. Correction for field nonuniformity in scintillation cameras through removal of spastial distortion. J Nucl Med. 1980 Aug;21(8):771-6.
16. Stoub EW, Colsher JG, Muehllehner G. Distortion correction method and apparatus for scintillation cameras. Patent US4298944 A. 1981.
17. Arseneau RE. Non-uniformity energy correction method and apparatus. Patent US4323977 A. 1982.
18. Arseneau RE. Dynamic threshold for scintillation camera. Patent US4475042 A. 1984.
19. Barfod JM. Gamma camera with image uniformity by energy correction offsets. Patent US4899054 A. 1990.
20. Spector SS, Brookeman VA, Kylstra CD, Diaz NJ. Analysis and correction of spatial distortions produced by the gamma camera. J Nucl Med. 1972 May;13(5):307-12.
21. Muehllehner G, Luig H. Septal penetration in scintillation camera collimators. Phys Med Biol. 1973 Nov;18(6):855-62.
22. Muehllehner G. Radiation imaging device. Patent US3745345 A. 1973.
23. Bertelsen H. Gamma camera with automatc adjustment of the energy spectrum. Patent US6635878 B2. 2003.
24. Richey JB, Wake RH, Wilson HH, Cheiky MC. Dynamic uniform flood correction for radioisotope cameras. Patent US4151416 A. 1979.
25. Tararine M. Method for correcting the uniformity of a gamma camera. Patent US5606166 A. 1997.
26. Kaviani S, Zeraatkar N, Sajedi S, Akbarzadeh A, Gorjizadeh N, Farahani MH, Teimourian B, Ghafarian P, Sabet H, Ay MR. Design and development of a dedicated portable gamma camera system for intra-operative imaging. Phys Med. 2016 Jul;32(7):889-97.
27. Ay M, Arabi H, Farahani M, Zeraatkar N, Sarkar S, Sajedi S, Naderi Rastgar N, Ghafarian P. SurgeoSight™: An Intraoprative hand held gamma camera for precise localization of sentinel lymph nodes. Eur J Nucl Med Mol Imaging. 2012;39(Suppl 2):S385.

28. Gorjizadeh N, Zeraatkar N, Kaviani A, Far SF, Farahani M, Akbarzadeh A, Sajedi S, Teimourian B, Ay M. Performance Evaluation of a small field of view portable gamma camera for localization of sentinel lymph nodes. Eur J Nucl Med Mol Imaging. 2013;40(Suppl 2):S99.

29. Grau V, Mewes AU, Alcañiz M, Kikinis R, Warfield SK. Improved watershed transform for medical image segmentation using prior information. IEEE Trans Med Imaging. 2004 Apr;23(4):447-58.

30. Bookstein FL. Principal warps: thin-plate splines and the decomposition of deformations. IEEE Trans Pattern Anal Mach Intell. 1989;11(6):567-85.

31. Kohonen T. The self-organizing map. Proc IEEE. 1990;78(9):1464-80.

32. Cottrell M, Olteanu M, Rossi F, Villa-Vialaneix N. Theoretical and applied aspects of the self-organizing maps. In: Merényi E, Mendenhall JM, O'Driscoll P, editors. Advances in self-organizing maps and learning vector quantization. Switzerland: Springer International Publishing; 2016. p. 3-26.

33. de Bodt E, Cottrell M, Verleysen M. Statistical tools to assess the reliability of self-organizing maps. Neural Netw. 2002 Oct-Nov;15(8-9):967-78.

34. Erwin E, Obermayer K, Schulten K. Self-organizing maps: ordering, convergence properties and energy functions. Biol Cybern. 1992;67(1):47-55.

35. Tolat VV. An analysis of Kohonen's self-organizing maps using a system of energy functions. Biol Cybern. 1990;64(2):155-64.

36. Palomares SE. Calibration of monolithic crystal-based detectors. Patent US20150276953 A1. 2015.

37. National Electrical Manufacturers Association. NEMA standards publication NU 1-2007: Performance measurements of gamma cameras, 2007.

38. Levin CS, Hoffman EJ, Tomai MP, MacDonald LR. PSPMT and photodiode designs of a small scintillation camera for imaging malignant breast tumors. IEEE Trans Nucl Sci. 1997;44(4):1513-20.

39. David S, Georgiou M, Fysikopoulos E, Belcari N, Loudos G. Imaging performance of silicon photomultipliers coupled to BGO and CsI:Na arrays. J Instrum. 2013;8(12):P12008.

40. Deprez K, Van Holen R, Vandenberghe S. A high resolution SPECT detector based on thin continuous LYSO. Phys Med Biol. 2014 Jan 6;59(1):153-71.

41. Bouckaert C, Marcinkowski R, Deprez K, Espana Palomares S, Van Holen R, Vandenberghe S. Optimization of digital silicon photomultipliers for monolithic SPECT scintillators. J Nucl Med. 2013;54(Suppl 2):2160.

42. Ferretti A, Chondrogiannis S, Marcolongo A, Rubello D. Phantom study of a new hand-held γ-imaging probe for radio-guided surgery. Nucl Med Commun. 2013 Jan;34(1):86-90.